Composites Science and Technology 70 (2010) 1023–1030

Contents lists available at ScienceDirect

Composites Science and Technology

journal homepage: www.elsevier.com/locate/compscitech

Indentation of a laminated composite plate with an interlayer rectangular void

W. Jiang, R.C. Batra *

Department of Engineering Science and Mechanics, M/C 0219, Virginia Polytechnic Institute & State University, Blacksburg, VA 24061, USA

ARTICLE INFO

Article history:
Received 3 January 2010
Received in revised form 25 February 2010
Accepted 27 February 2010
Available online 4 March 2010

Keywords:
Indentation
A. Laminate
C. Computational mechanics
B. Voids
C. Anisotropy

ABSTRACT

We employ the Eshelby–Stroh formalism to study generalized plane strain infinitesimal deformations caused due to the indentation by a rigid circular cylinder of an elastic laminated plate with a through-the-width rectangular void between two adjoining layers. Assuming that the void does not close during the indentation process, we find the indentation modulus (i.e., the slope of the indentation load vs. the indentation depth curve) as a function of the void size, the void position, elastic moduli of the layers, and boundary conditions at the edges. The change in the indentation modulus caused by an interlayer void parallel to the major surfaces of an anisotropic plate can potentially be used to estimate the void size and location.

1. Introduction

Due to their high specific stiffness and specific strength, composite are being increasingly used in numerous engineering applications. However, mechanical properties of composites may degrade severely with repeated impact and cyclic loading. Failures of structures, particularly aircraft structures, often have tragic consequences. Applications of composites tend to be limited or inhibited by the lack of long-term service experience and the difficulty to accurately quantify damage and thus determine the remaining useful life of the structure. Damage detection techniques such as thermal deplying and optical microscopy require either the partial or the total destruction of the structural component [2]. Most conventional nondestructive evaluation techniques such as ultrasonic C-scan, X-ray, thermography and eddy current have limited applications as they require a structural component to be taken out of service for a substantial length of time for damage inspection and assessment. Global damage detection methods [3], based on the assumption that a change in physical properties of a structure alters its modal characteristics, have also been developed. These methods either depend on analytical models or prior test data for the detection and the location of damage or on the output from several sensors bonded to the structure. Technical issues that need to be considered during *in situ* monitoring of structures include the following: surface-bonded resistive strain gauges are susceptible to electromagnetic and electrical interference in addition to physical damage, and the acoustic emission suffers from low signal-to-noise ratio. Sometimes it is advisable to simultaneously use two or more techniques and synthesize their outputs to quantitatively and qualitatively ascertain the damage type, its extent and location.

Damages in fiber-reinforced composites include fiber breakage, fiber kinking, fiber buckling, fiber/matrix debonding, matrix cracking, delamination, and fiber and matrix crushing. A composite structure under complex loading will have several narrow cracks oriented in different directions and located at various points. Here we focus on studying a technique to detect the separation (or the delamination) between two adjoining layers. We study a model problem involving the indentation by a rigid circular cylinder of a flat elastic laminated plate with a through-the-width rectangular void between two adjoining layers composed of anisotropic and homogeneous materials. We assume that the indentation load is small enough not to close the void. The indentation test has been used to determine mechanical properties of materials. It is commonly believed that the indentation load vs. the indentation depth response during unloading corresponds to elastic deformations of the indented material. The indentation modulus, i.e., the slope of the indentation load vs. the indentation depth curve for infinitesimal deformations, is a function of elastic properties of the structure (e.g., see [11]). Therefore, the degradation in elastic properties due to voids will decrease the indentation modulus, and the change will depend upon the number of voids, their locations, and their sizes. Thus one should be able to use the indentation modulus to estimate voids in a composite. We have reviewed the literature on indentation problems in [1] and thus omit it here for the sake of brevity.

We assume that a plane strain state of deformation prevails in the laminate, the void does not close during the indentation process, and employ the Eshelby–Stroh formalism to find infinitesimal

* Corresponding author.
E-mail addresses: wjiang@vt.edu (W. Jiang), rbatra@vt.edu (R.C. Batra).

0266-3538/$ - see front matter © 2010 Elsevier Ltd. All rights reserved.
doi:10.1016/j.compscitech.2010.02.030

deformations of the laminate. The plane strain assumption requires a through-the-width void which can be detected visually. The goal here is to use the Eshelby–Stroh formalism to analyze the problem, and quantify changes in the indentation modulus as a function of the location and the length of the void, and other material and geometric parameters. For voids completely in the interior of a structure one needs to study three-dimensional deformations, and for narrow voids or cracks one should allow for closing of void surfaces which will suddenly increase the indentation modulus. This latter problem is more challenging than the one studied here since one needs to satisfy the non-interpenetration of the material across the just generated closed surface, track closing of the void with an increase in the indentation load, and permit sliding between the contacting surfaces; it will be studied in future.

2. Problem formulation

Fig. 1 depicts a schematic sketch of the generalized plane strain problem involving the indentation of a two-layer composite plate by a smooth rigid circular cylinder. The through-the-width void of length $2b$ and thickness h_b is in the x_1x_3 – plane. It is assumed that the length of the void, of the cylinder and of the layer in the x_2 – direction (perpendicular to the plane of the paper) is very large as compared to the length L and the thickness $h = w_1 + w_2$ of the plate. Here w_1 and w_2 are thicknesses of the layers above and below the void. We denote the indentation depth by u_0, and the semi-contact width by c. Prior to the indentation, the centers of the contact area and the void are, respectively, at (x_c, h) and (x_b, w_2). The words "crack" and "void" are used interchangeably.

In the absence of body forces, equations in rectangular Cartesian coordinates governing deformations of the layer are

$$\sigma_{ij,j} = 0, \; i, \; j = 1, 2, 3, \tag{1}$$

$$\sigma_{ij} = C_{ijkl}e_{kl}, \quad C_{ijkl} = C_{jikl} = C_{klij}, \tag{2}$$

$$e_{kl} = \frac{1}{2}(u_{k,l} + u_{l,k}), \tag{3}$$

where $\sigma_{ij} = \sigma_{ji}$ is the Cauchy stress tensor, $\sigma_{ij,j} = \partial\sigma_{ij}/\partial x_j$, a repeated index implies summation over the range of the index, e_{kl} the infinitesimal strain tensor, u_i the displacement of a point in the x_i-direction, and C_{ijkl} is an elastic constant of the material of the linear elastic layer. Symmetries indicated in Eq. (2) imply that, for a three-dimensional problem, C_{ijkl} can be written as a symmetric 6×6 matrix, and σ_{ij} and e_{kl} as 6×1 matrices.

Boundary conditions on the top surface of the layer are:

$$\sigma_{13} = \sigma_{33} = 0 \quad \text{on } x_3 = h \quad \text{and} \quad |x_1 - L/2| > c, \tag{4.1}$$

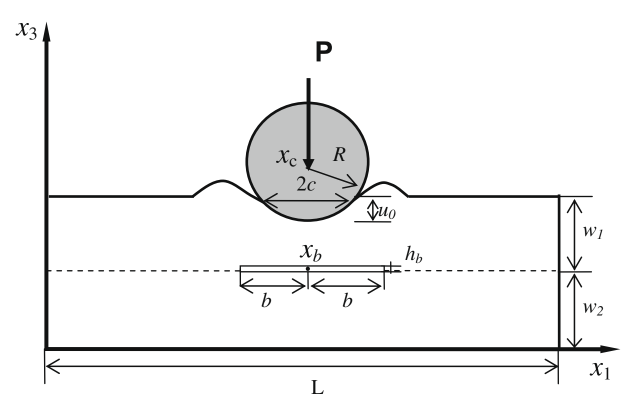

Fig. 1. Schematic sketch of the problem studied.

$$\sigma_{11}\sin\theta\cos\theta - \sigma_{31}\cos 2\theta - \sigma_{33}\sin\theta\cos\theta = 0,$$
$$u_3 = R - u_0 - \sqrt{R^2 - (x_1 - L/2)^2} \text{ on } x_3 = h \quad \text{and}$$
$$|x_1 - L/2| \leqslant c. \tag{4.2}$$

Here $\theta = \arcsin((x_1 - L/2)/R)$. In cylindrical coordinates, the left-hand side of Eq. $(4.2)_1$ equals the tangential traction $\sigma_{r\theta}$ at a point on the contact surface, and at points of the contact surface not contacting the indenter, $\sigma_{rr} \geqslant 0$. We assume that there is no separation between the indenter and the deformable layer; thus the contact surface is contiguous.

The layer is either taken to be (i) fixed at the edges $x_1 = 0, L$ and traction free at the bottom surface $x_3 = 0$; or (ii) fixed at $x_3 = 0$ and traction free at $x_1 = 0, L$. Boundary conditions at a fixed edge are

$$u_1 = u_3 = 0, \tag{5}$$

and those at a traction free surface are

$$\sigma_{ij}n_j = 0 \tag{6}$$

where $\mathbf{n}$ is the unit normal vector to the free surface.

We assume that the void does not close during the indentation process; thus void surfaces are taken to be traction free and boundary conditions (6) are applied on them. This restricts the indentation load or the indentation depth considered in the problem but does not affect the goal of the work in quantifying the change in the indentation modulus caused by the presence of voids.

The axial load P per unit length of the cylinder, or the indentation load, is calculated from

$$P = -\int_{L/2-c}^{L/2+c} (\sigma_{33} - \sigma_{13}\tan\theta)dx_1. \tag{7}$$

If the bottom surface is fixed, the indentation depth equals the absolute value of the vertical displacement of the point of intersection of the centroidal axis of the cylinder and the top surface of the plate. However, when the bottom surface is traction free then the indentation depth equals the difference in the vertical displacements of points of intersection of the centroidal axis of the cylinder and the top and the bottom surfaces of the plate.

3. Analytical solution of the problem

We assume that the displacement field $\mathbf{u}$ and hence stresses and strains induced in the plate are functions of x_1 and x_3 only, and write a general solution of Eqs. (1)–(3) as follows by using Stroh's formalism [7]:

$$\mathbf{u} = \sum_{\alpha=1}^{3}[\mathbf{a}_\alpha f_\alpha(z_\alpha) + \bar{\mathbf{a}}_\alpha f_{\alpha+3}(\bar{z}_\alpha)], \tag{8}$$

$$\boldsymbol{\sigma}_1 = -\sum_{\alpha=1}^{3}[p_\alpha \mathbf{b}_\alpha f'_\alpha(z_\alpha) + \bar{p}_\alpha \bar{\mathbf{b}}_\alpha f'_{\alpha+3}(\bar{z}_\alpha)], \tag{9}$$

$$\boldsymbol{\sigma}_3 = -\sum_{\alpha=1}^{3}[\mathbf{b}_\alpha f'_\alpha(z_\alpha) + \bar{\mathbf{b}}_\alpha f'_{\alpha+3}(\bar{z}_\alpha)], \tag{10}$$

where

$$(\boldsymbol{\sigma}_1)_i = \sigma_{i1}, \quad (\boldsymbol{\sigma}_3)_i = \sigma_{i3}. \tag{11}$$

Furthermore, f_α $(\alpha = 1, 2, 3)$ are arbitrary analytic functions of z_α, $z_\alpha = x_1 + p_\alpha x_3$, $\bar{z}_\alpha$ is complex conjugate of z_α, f'_α denotes the derivative of f_α with respect to z_α, p is an eigenvalue, and $\mathbf{a}$ and $\mathbf{b}$ are the corresponding eigenvectors of the following eigenvalue problem:

$$\mathbf{N}\zeta = p\zeta, \tag{12}$$

$$\mathbf{N} = \begin{bmatrix} -\mathbf{T}^{-1}\mathbf{R}^{\mathrm{T}} & \mathbf{T}^{-1} \\ \mathbf{R}\mathbf{T}^{-1}\mathbf{R}^{\mathrm{T}} - \mathbf{Q} & -\mathbf{R}\mathbf{T}^{-1} \end{bmatrix}, \quad \zeta = \begin{Bmatrix} \mathbf{a} \\ \mathbf{b} \end{Bmatrix}, \tag{13}$$

$$Q_{il} = C_{i11l}, \quad R_{il} = C_{i13l}, \quad T_{il} = C_{i33l}. \tag{14}$$

For the strain energy density to be positive definite, p must be complex. Let (p_α, a_α), $\alpha = 1, 2, \ldots, 6$ be eigensolutions of Eq. (12) such that

$$\mathrm{Im}(p_\alpha) > 0, \quad p_{\alpha+3} = \bar{p}_\alpha, \quad a_{\alpha+3} = \bar{a}_\alpha, \quad \alpha = 1, 2, 3, \tag{15}$$

where $\bar{p}_\alpha$ is the complex conjugate of p_α. The general solution (8)–(10) holds even when the six eigenvalues are not distinct but there exist six linearly independent eigenvectors. Ting [9] has discussed how to modify the general solution when the eigenvalue problem defined by Eqs. (12)–(14) does not have six linearly independent eigenvectors; e.g. for an isotropic material.

As was done to study the indentation of an undamaged medium [1], we separate the entire domain into several regions; the number of subregions depends upon the contact zone and the void area as depicted in Fig. 2. In order to satisfy boundary conditions and continuity conditions at interfaces between adjoining subregions, we assume the following series solution for the nth ($n = 1, 2, 3\ldots$) region.

$$\begin{aligned} f_\alpha^{(n)}\left(z_\alpha^{(n)}\right) &= d_\alpha^{(n)} \exp\left(\lambda_{0\alpha}^{(n)} z_\alpha^{(n)}\right) + e_\alpha^{(n)} \exp\left(\lambda_{0\alpha}^{(n)}\left(p_\alpha^{(n)} h - z_\alpha^{(n)}\right)\right) \\ &+ v_\alpha^{(n)} \exp\left(\eta_{0\alpha}^{(n)} z_\alpha^{(n)}\right) + w_\alpha^{(n)} \exp\left(\eta_{0\alpha}^{(n)}\left(l^{(n)} - z_\alpha^{(n)}\right)\right) \\ &+ \sum_{k=1}^{\infty}\left\{q_{k\alpha}^{(n)} \exp\left(\lambda_{k\alpha}^{(n)} z_\alpha^{(n)}\right) + r_{k\alpha}^{(n)} \exp\left(\lambda_{k\alpha}^{(n)}\left(p_\alpha^{(n)} h - z_\alpha^{(n)}\right)\right)\right\} \\ &+ \sum_{m=1}^{\infty}\left\{s_{m\alpha}^{(n)} \exp\left(\eta_{m\alpha}^{(n)} z_\alpha^{(n)}\right) + t_{m\alpha}^{(n)} \exp\left(\eta_{m\alpha}^{(n)}\left(l^{(n)} - z_\alpha^{(n)}\right)\right)\right\}, \\ &0 \leqslant x_1^{(n)} \leqslant l^{(n)}, \end{aligned} \tag{16}$$

where

$$\begin{aligned} &z_\alpha^{(n)} = x_1^{(n)} + p_\alpha^{(n)} x_3^{(n)}, \quad \lambda_{0\alpha}^{(n)} = \frac{\pi i}{2l}, \quad \lambda_{k\alpha}^{(n)} = \frac{k\pi i}{l^{(n)}}, \\ &\eta_{0\alpha}^{(n)} = -\frac{\pi i}{2p_\alpha h}, \quad \eta_{m\alpha}^{(n)} = -\frac{m\pi i}{p_\alpha^{(n)} h}, \quad i = \sqrt{-1}. \end{aligned} \tag{17}$$

Following the work presented in [10], we assume that the unknowns $d_\alpha^{(n)}$, $e_\alpha^{(n)}$, $v_\alpha^{(n)}$ and $w_\alpha^{(n)}$ are real while $q_{k\alpha}^{(n)}$, $r_{k\alpha}^{(n)}$, $s_{m\alpha}^{(n)}$ and $t_{m\alpha}^{(n)}$ are complex; these will be determined from boundary conditions, and continuity conditions at the interfaces. In Eqs. (16) and (17), $l^{(n)}$ ($n = 1, 2, 3\ldots$) is the length of the nth segment, and $x_1^{(n)}$ is the x_1 – coordinate of a point in the nth segment measured from the left edge of the segment. Note that each term in series (16) is an analytical function of $z_\alpha^{(n)}$. The function $\exp(\lambda_{k\alpha}^{(n)} z_\alpha^{(n)})$ varies sinusoidally on the surface $x_3^{(n)} = 0$ and decays exponentially in the $x_\alpha^{(n)}$-direction. With increasing k, higher harmonics are introduced on the surface $x_3^{(n)} = 0$ accompanied by steeper exponential decay in the $x_3^{(n)}$-direction. Similarly, functions multiplying $r_{k\alpha}^{(n)}, s_{m\alpha}^{(n)}$ and $t_{m\alpha}^{(n)}$ vary sinusoidally on surfaces $x_3^{(n)} = h^{(n)}$, $x_1^{(n)} = 0$ and $x_1^{(n)} = L$, respectively. The inequality $(15)_1$ ensures that all functions decay exponentially towards the interior of the layer. The polynomial terms in $z_\alpha^{(n)}$ are introduced to play the role of the constant in the Fourier series expansion on the four bounding surfaces. The choice $f_{\alpha+3}^{(n)}(\bar{z}_\alpha^{(n)})$ equal to the complex conjugate of $f_\alpha^{(n)}(z_\alpha^{(n)})$ ensures that displacements and stresses are real.

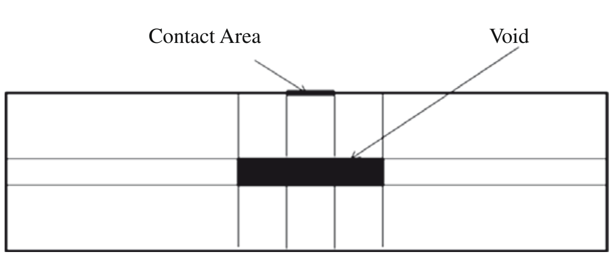

Fig. 2. Schematic sketch of the partition of a laminate into several zones.

Substituting for $f_\alpha(z_\alpha)$ from Eq. (16) into Eqs. (8)–(10), we get the following for the displacements $\mathbf{u}^{(n)}$ and stresses $\boldsymbol{\sigma}_1^{(n)}$ and $\boldsymbol{\sigma}_3^{(n)}$ in the nth segment:

$$\begin{aligned} \mathbf{u}^{(n)} = \mathbf{A}\Big\{&\left\langle \exp\left(\beta_{0^*}^{(n)}\right)\right\rangle \mathbf{d}^{(n)} + \left\langle \exp\left(\gamma_{0^*}^{(n)}\right)\right\rangle \mathbf{e}^{(n)} \\ &+ \sum_{k=1}^{\infty}\left[\left\langle \exp\left(\beta_{k^*}^{(n)}\right)\right\rangle \mathbf{q}_k^{(n)} + \left\langle \exp\left(\gamma_{k^*}^{(n)}\right)\right\rangle \mathbf{r}_k^{(n)}\right] \\ &+ \left\langle \exp\left(\delta_{0^*}^{(n)}\right)\right\rangle \mathbf{v}^{(n)} + \left\langle \exp\left(\xi_{0^*}^{(n)}\right)\right\rangle \mathbf{w}^{(n)} \\ &+ \sum_{m=1}^{\infty}\left[\left\langle \exp\left(\delta_{m^*}^{(n)}\right)\right\rangle \mathbf{s}_m^{(n)} + \left\langle \exp\left(\xi_{m^*}^{(n)}\right)\right\rangle \mathbf{t}_k^{(n)}\right]\Big\} + \text{conjugate}, \end{aligned} \tag{18}$$

$$\begin{aligned} \boldsymbol{\sigma}_1^{(n)} = \mathbf{B}\Big\{&-\left\langle \lambda_{0^*}^{(n)} p_*^{(n)} \exp\left(\beta_{0^*}^{(n)}\right)\right\rangle \mathbf{d}^{(n)} \\ &+ \left\langle \lambda_{0^*}^{(n)} p_*^{(n)} \exp\left(\gamma_{0^*}^{(n)}\right)\right\rangle \mathbf{e}^{(n)} - \left\langle \eta_{0^*}^{(n)} p_*^{(n)} \exp\left(\delta_{0^*}^{(n)}\right)\right\rangle \mathbf{v}^{(n)} \\ &+ \left\langle \eta_{0^*}^{(n)} p_*^{(n)} \exp\left(\xi_{0^*}^{(n)}\right)\right\rangle \mathbf{w}^{(n)} + \sum_{k=1}^{\infty}\Big[-\left\langle \lambda_{k^*}^{(n)} p_*^{(n)} \exp\left(\beta_{k^*}^{(n)}\right)\right\rangle \mathbf{q}_k^{(n)} \\ &+ \left\langle \lambda_{k^*}^{(n)} p_*^{(n)} \exp\left(\gamma_{k^*}^{(n)}\right)\right\rangle \mathbf{r}_k^{(n)}\Big] + \sum_{m=1}^{\infty}\Big[-\left\langle \eta_{m^*}^{(n)} p_*^{(n)} \exp\left(\delta_{m^*}^{(n)}\right)\right\rangle \mathbf{s}_m^{(n)} \\ &+ \left\langle \eta_{m^*}^{(n)} p_*^{(n)} \exp\left(\xi_{m^*}^{(n)}\right)\right\rangle \mathbf{t}_k^{(n)}\Big]\Big\} + \text{conjugate}, \end{aligned} \tag{19}$$

$$\begin{aligned} \boldsymbol{\sigma}_3^{(n)} = \mathbf{B}\Big\{&\left\langle \lambda_{0^*}^{(n)} \exp\left(\beta_{0^*}^{(n)}\right)\right\rangle \mathbf{d}^{(n)} - \left\langle \lambda_{0^*}^{(n)} \exp\left(\gamma_{0^*}^{(n)}\right)\right\rangle \mathbf{e}^{(n)} \\ &+ \sum_{k=1}^{\infty}\left[\left\langle \lambda_{k^*}^{(n)} \exp\left(\beta_{k^*}^{(n)}\right)\right\rangle \mathbf{q}_k^{(n)} - \left\langle \lambda_{k^*}^{(n)} \exp\left(\gamma_{k^*}^{(n)}\right)\right\rangle \mathbf{r}_k^{(n)}\right] \\ &+ \left\langle \eta_{0^*}^{(n)} \exp\left(\delta_{0^*}^{(n)}\right)\right\rangle \mathbf{v}^{(n)} - \left\langle \eta_{0^*}^{(n)} \exp\left(\xi_{0^*}^{(n)}\right)\right\rangle \mathbf{w}^{(n)} \\ &+ \sum_{m=1}^{\infty}\left[\left\langle \eta_{m^*}^{(n)} \exp\left(\delta_{m^*}^{(n)}\right)\right\rangle \mathbf{s}_m^{(n)} - \left\langle \eta_{m^*}^{(n)} \exp\left(\xi_{m^*}^{(n)}\right)\right\rangle \mathbf{t}_k^{(n)}\right]\Big\} + \text{conjugate}, \end{aligned} \tag{20}$$

where

$$\begin{aligned} &\mathbf{A} = [\mathbf{a}_1\mathbf{a}_2\mathbf{a}_3], \quad \mathbf{B} = [\mathbf{b}_1\mathbf{b}_2\mathbf{b}_3], \\ &\beta_{k\alpha}^{(n)} = \lambda_{k\alpha}^{(n)} z_\alpha^{(n)}, \quad \gamma_{k\alpha}^{(n)} = \lambda_{k\alpha}^{(n)}(p_\alpha^{(n)} h - z_\alpha^{(n)}), \\ &\delta_{m\alpha}^{(n)} = \eta_{m\alpha}^{(n)} z_\alpha^{(n)}, \quad \xi_{m\alpha}^{(n)} = \eta_{m\alpha}^{(n)}(l^{(n)} - z_\alpha^{(n)}), \\ &\langle \phi_* \psi_* \chi_* \rangle = \mathrm{diag}[\phi_1\psi_1\chi_1, \phi_2\psi_2\chi_2, \phi_3\psi_3\chi_3], \\ &\left(\mathbf{d}^{(n)}\right)_\alpha = d_\alpha^{(n)}, \quad \alpha = 1, 2, 3. \end{aligned} \tag{21}$$

Substitution from Eqs. (18)–(20) into boundary conditions and continuity conditions at the interfaces between adjoining regions gives a system of linear algebraic equations whose solution gives unknowns $\mathbf{d}^{(n)}$, $\mathbf{v}^{(n)}$, $\mathbf{w}^{(n)}$, $\mathbf{q}_k^{(n)}$, $\mathbf{r}_k^{(n)}$, $\mathbf{s}_m^{(n)}$ and $\mathbf{t}_m^{(n)}$ ($n = 1, 2, 3$; $k = 0,1,2\ldots$; $m = 0,1,2\ldots$). We note that boundary conditions are satisfied on the average as is done in the method of Fourier series. Furthermore, boundary condition $(4.2)_2$ is first differentiated with respect to x_1 to eliminate u_0 before it is imposed. In order to maintain approximately the same period of the largest harmonic on all interfaces and boundaries, we truncate k to $K^{(n)}$ and m to $M^{(n)}$ for the nth segment with

$$K^{(n)} = \mathrm{Ceil}\left(K\frac{l^{(n)}}{L}\right), \quad M^{(n)} = \mathrm{Ceil}\left(K\frac{h^{(n)}}{L}\right) \tag{22}$$

where Ceil($*$) gives the smallest integer greater than or equal to $*$, and K is the pre-determined number of terms.

As pointed in [10], we note from the structure of the solution (18)–(20) that the component functions decrease exponentially from the boundary/interfaces into the interior of the nth lamina. By truncating the series, we have effectively ignored coefficients with suffices greater than a particular value and approximated the coefficients which have small suffices. Due to the rapid decay of component functions associated with large suffices, the truncation of the series will not greatly influence the solution at the interior points. A larger value of K will give a more accurate solution at points close to the boundary and interfaces. It should also be noted that the coefficients $q_k^{(n)}$ and $r_k^{(n)}$ in (19), (20) are multiplied by $\lambda_k^{(n)}$ while $s_m^{(n)}$ and $t_m^{(n)}$ are multiplied by $\eta_{m^*}^{(n)}$, thus indicating that the stresses will converge more slowly than the displacements.

4. Verification of the solution technique

The composite plate is divided into several small portions as shown in Fig. 2 to satisfy boundary conditions on the void surfaces and at the contact region. In order to compute a solution within acceptable errors, $K^{(n)}$ and $M^{(n)}$ should be kept large even for these small layers. Thus the total number K of equations may become very large. We have developed a computer code in Fortran to solve a large system of simultaneous linear algebraic equations by using the PARDISO package in Intel® Math Kernel Library.

The Eshelby–Stroh formalism adopted here is similar to that employed in [10,12–14] wherein infinitesimal static deformations of elastic laminated composites were studied and it was shown that the technique satisfies very well the continuity of tractions and displacements across interfaces between two adjoining layers. The methodology was applied in [1] to study the indentation of a homogeneous material. Thus we only need to ensure that the technique captures well singularities at the corners of a rectangular void. For completeness we first compare presently computed results with those available in the literature for an indentation problem that does not involve any stress singularities and then for a problem that involves singularities.

The first problem analyzed here is the same as that studied analytically in [4] and involves the indentation of a homogeneous orthotropic half-space by the smooth rigid parabolic indenter, $x_3 = \frac{(x_1-L/2)^2}{2R}$, where R is the radius of curvature of the indenter at the point $(L/2, 0)$. Values assigned to various material and geometric parameters are listed below.

$$\begin{aligned}&E_1 = 25.0\ \text{GPa}, \quad E_2 = E_3 = 1.0\ \text{GPa}, \quad G_{23} = 0.2\ \text{GPa},\\ &G_{12} = G_{31} = 0.5\ \text{GPa}, \quad \nu_{12} = \nu_{23} = \nu_{13} = 0.25,\\ &L = 1.0\ \text{m}, \quad h = 0.4\ \text{m}, \quad R = 1.0\ \text{m}, \quad 2c = 0.04\ \text{m}.\end{aligned} \tag{23}$$

Relations $E_i/\nu_{ij} = E_j/\nu_{ji}$ (no sum on i and j) and values of parameters listed in Eq. (23) give $\nu_{21} = \nu_{31} = 0.01$ and $\nu_{32} = 0.25$. Note that $E_2 = E_3$ does not imply that the material must be transversely isotropic with the axis of transverse isotropy along the x_1-axis. These values of elastic parameters are such that the 6×6 matrix of elastic constants is positive definite, i.e., the six eigenvalues of this matrix are positive. Thus a boundary-value problem with displacements prescribed on a part of the boundary will have a unique solution. We should also add that values of elastic constants listed in Eq. (23) are for a typical composite rather than for a specific fiber-reinforced material. We have compared in Fig. 3 the pressure distribution on the contact surface obtained from the analytical solution of [4] with that computed by using the present method in which the entire laminate is divided into 15 layers and K is set equal to 1000 in the series solution represented by Eqs. (18)–(20). It is clear that the two pressure distributions agree well with each other, and the maximum error in the pressure computed over the region $(x_1 - L/2) < 0.9c$ is 5.2%.

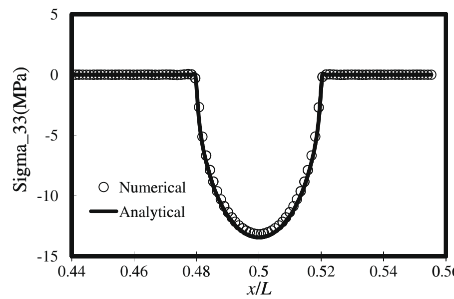

Fig. 3. For a homogeneous layer, comparison of the presently computed pressure distribution on the contact surface with that of Hwu and Fan [4].

In order to ensure accuracy of the computed stresses near the void corners we analyze deformations of an infinite plate made of an isotropic material with a rectangular hole at its center and in-plane surface tractions applied at infinity, and compare our results with those of [5] who used both the conformal mapping technique to solve the problem analytically and the finite element method to analyze it numerically. As mentioned above, Ting [8] has discussed techniques to modify the Eshelby–Stroh formalism for solving boundary-value problems for isotropic materials. Here, however, we alter values of elastic constants by ±1% to get unequal eigenvalues of the problem defined by Eq. (12). We used 1000 terms, the same as for the contact problem described above, to get a converged solution. Results for an infinite plate truncated to 30×30 m with $(2b \times h_b) = (l \times w) = (3 \times 1\ \text{m})$ rectangular hole at its centroid and subjected to uniform surface tractions q on the horizontal faces are compared with those of Lei et al. [5] in Fig. 4. It is evident that the two sets of results agree well with each other, and stress singularities at the void corners are well captured. Contour plots of stresses in Fig. 4c and d evince the stress concentration at the hole corners.

5. Parametric study

We investigate the effect on the indentation modulus of the void size, the void position, material properties and boundary conditions. Unless otherwise noted, we have taken the center of the indenter at the point $(L/2, R + h)$, the center of the void at the point (x_b, w_2), values of material parameters listed in Eq. (23), $2b = 0.2$ m, $h_b = 2$ mm, and the composite plate is fixed at the bottom surface and traction free at the left and the right edges. The void length, $2b$, is specified for each case studied. We note that $2b/L = 0.2$ and $h_b/h = 0.05$. For every problem studied below, we checked our solution to ensure that the void did not close during the indentation process. Also, "no damage" in Figs. stands for "no interlayer void".

5.1. Void size

With, $w_1 = w_2$ the center of the void at the point $(L/2, h/2)$ and for void lengths varying from 0 (no damage) to 0.2 m, we have plotted in Fig. 5 the indentation load vs. the indentation depth curves. It is clear that the indentation modulus decreases noticeably with an increase in the void length. For indentation depth of 2 mm, and void lengths of 0.1 m, 0.15 m, and 0.2 m, the indentation load drops, respectively, to 75%, 60%, and 50% of the indentation load for the undamaged layer. The 25% reduction in the indentation load for void length of 0.1 m is very large, and the

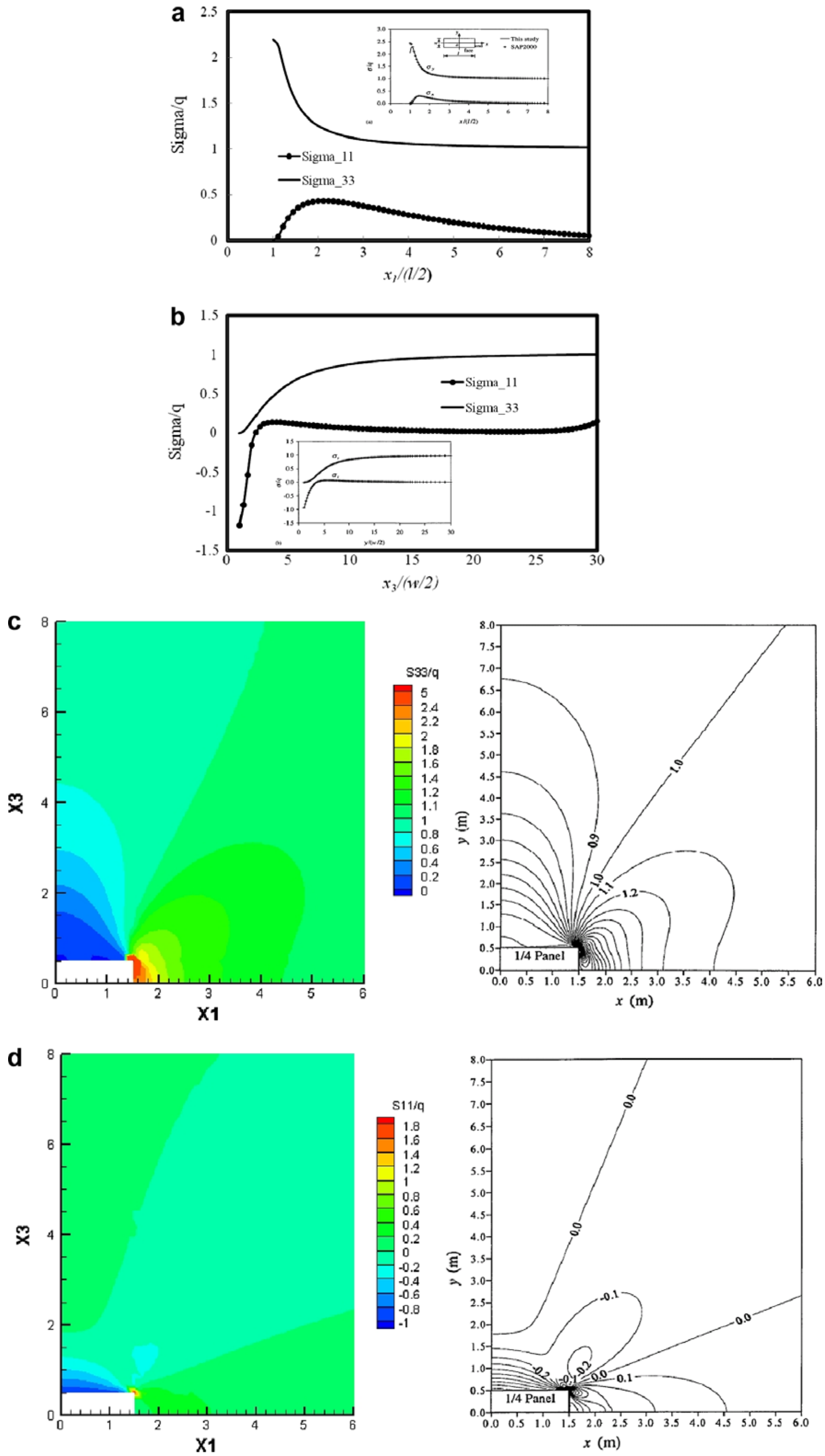

Fig. 4. Stress distribution around a 3 m × 1 m rectangular hole at the centroid of the 30 m × 30 m plate made of an isotropic linear elastic material and subjected to an uniaxial traction q at the two horizontal boundary surfaces: (a) stresses along the horizontal line passing through the corner, (b) stresses along the vertical line passing through the corner, (c) and (d) contour plots of the stresses (right figs. from [5] and left figs. present results) normalized by the applied traction q. Insets in (a) and (b) denote results (indicated by SAP2000) reported in [5] by using the finite element method.

reduction will decrease with a decrease in the void size. The sensitivity of the instrument will determine how accurately one can measure the indentation load and the indentation depth. Thus, in principle, results of the indentation test can be used to detect and possibly quantify the presence of a through-the-width void in a laminated composite.

5.2. Void position

For a void of length $2b = 0.15$ m, Fig. 6 exhibits the indentation load vs. the indentation depth curves for four locations of the void below the indenter which is accomplished by changing the thicknesses, w_1 and w_2, of the upper and the lower layers but keeping

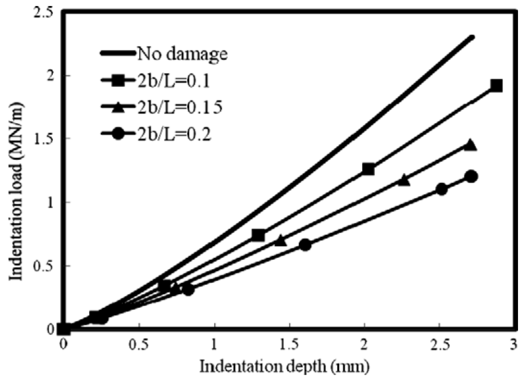

Fig. 5. Effect of the void length, $2b$, on the indentation load vs. the indentation depth curves for a composite layer with points on the bottom surface held fixed.

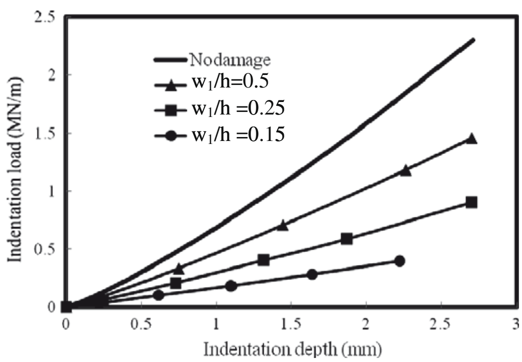

Fig. 6. For different vertical distances of the void below the indenter, the indentation load vs. the indentation depth curves for a laminated composite with points on the bottom surface of composite restrained from moving.

the total thickness h constant. As the void location moves towards the indenter, the indentation load for the same indentation depth drops rapidly.

For the void center located at $x_b = 0.5$ m, 0.4 m and 0.3 m, results plotted in Fig. 7 show that for the two latter locations of the void center, the indentation load vs. the indentation depth curves are essentially the same as that for an undamaged layer, i.e., there were no void. For these two values of x_b the entire void lies to the left of the indenter center. From plots of Figs. 6 and 7 one can conclude that the indentation test is only effective in detecting voids located close to the indenter.

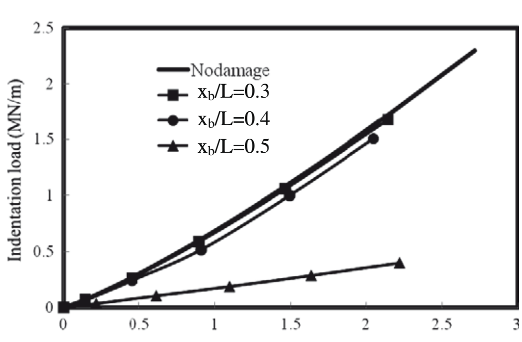

Fig. 7. For different locations of the void on the interface between the two layers, the indentation load vs. the indentation depth curves for a composite layer with points on the bottom surface having null displacements.

5.3. Material properties

It is shown in [1] that the two material parameters of the composite layer significantly influencing the indentation modulus are Young's modulus E_3 in the direction of indentation and the shear modulus G_{13} in the plane of deformation. For the void length $2b = 0.1$ m, the center of the void located at $(L/2, h/2)$, and different values of E_3 and G_{13} we have plotted in Figs. 8 and 9 the indentation load vs. the indentation depth. These results evince that the difference in the indentation load for a given indentation depth increases rapidly with an increase in the value of E_3 and a decrease in the value of G_{13}. Thus the indentation test can be readily used to find an inter-laminar void in a composite whose Young's modulus in the indentation direction is very large and the shear modulus G_{13} is very small.

5.4. Arrangement of layers

In Fig. 10 we have exhibited the indentation load vs. the indentation depth curves for five two-layer fiber-reinforced composite laminates. In each case, values of material parameters listed in Eq. (23) are with respect to the material principal axes, i.e., the rectangular Cartesian coordinate axes are aligned such that the x_1-axis is the fiber direction, and the x_3-axis is perpendicular to the lamina. Values of material parameters with respect to the global axes are obtained by using the tensor transformation rules. It is evident that the indentation modulus strongly depends upon the fiber orientation angle in the two layers. The presence of a rectangular void has virtually no effect on the indentation modulus for the 90°/90° laminas. However, for the 45°/90° composite the

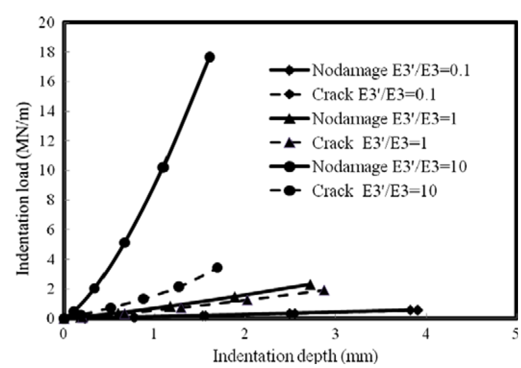

Fig. 8. For three values of Young's modulus in the transverse direction, the indentation load vs. the indentation depth curves of a laminated composite with points on the bottom surface rigidly clamped.

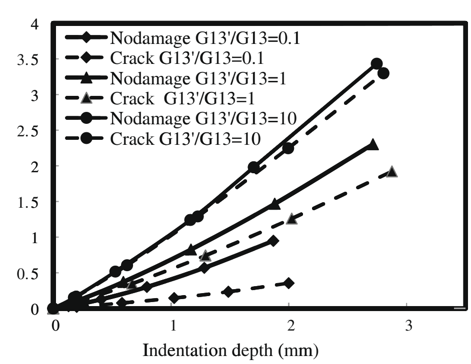

Fig. 9. For three values of the in-plane shear modulus, the indentation load vs. the indentation depth curves of a laminated composite with points on the bottom surface rigidly clamped.

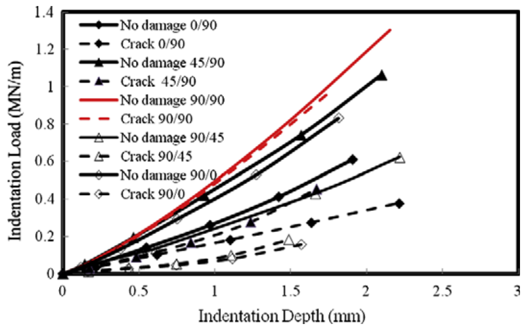

Fig. 10. For different two-layer composites with void locations on the interface between the two layers, the indentation load vs. the indentation depth curves for a composite layer with points on the bottom surface having null displacements ($w_1 = 0.1$ m, $w_2 = 0.1$ m). The first number in 45/90 gives the fiber orientation angle for the layer contacting the indenter.

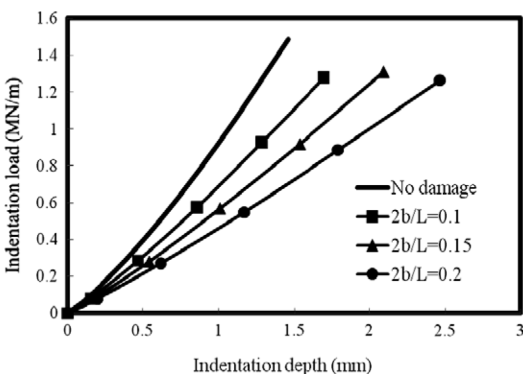

Fig. 11. For a two-layer laminated composite with clamped edges and bottom surface traction free, the indentation load vs. the indentation depth curves for three widths of the void.

indentation modulus drops noticeably because of the rectangular void at the interface between the two layers.

5.5. Boundary conditions

For a layer with the bottom surface perfectly bonded to a rigid surface, edges traction free, and three locations of the void, we have plotted in Fig. 11 the indentation load vs. the indentation depth curves. These results are qualitatively similar to those for a layer with edges clamped. For $b/L = 0.1$ and the indentation depth of 2 mm, the indentation load equals 1.1 MN/m when the edges are traction free and the bottom surface is fixed as opposed to 0.8 MN/m for the case of fixed edges and the bottom surface traction free. Results for different void positions, void sizes and material properties are not exhibited since they are also similar to those for a layer with clamped edges.

6. Discussion

We note that the indentation test is a well developed technique for determining mechanical properties of a material. By periodically finding the indentation modulus, the initiation and the growth of a void between two adjoining layers can be quantified. With sensitive instruments capable of measuring loads as small as a nano-Newton and indentations of about 1 nm, the accuracy and the reliability of the method can be enhanced. Furthermore, elastic deformations used to find the indentation modulus do not introduce any additional damage to the structure. Results presented herein are based on the assumption that the void does not close during the indentation process which tacitly applies to rather wide voids. For narrow voids (i.e., $h_b/h \ll 1$) either the indentation load will need to be very small for this assumption to be valid or the analysis will need to be modified to allow for the void to collapse. The closing of the void will be indicated by a sudden increase in the indentation modulus.

The goal of our work is to delineate the effect of various material and geometric parameters on the indentation modulus. Even though we have solved an idealized problem, results presented in the paper shed light on what parameters to focus on while using the indentation modulus for identifying damage in the structure.

As stated in [6] the damage identification involves determining the existence of damage, its geometric location, its severity or magnitude, and prediction of the remaining service life of the structure. The present work partially addresses the first three issues but sheds no light on the durability of structures. By conducting several numerical simulations, one can establish a functional relationship between the change in the indentation modulus and other variables such as the void length, the void location, and values of material and geometric parameters.

We note that results presented herein are not applicable to the indentation of laminated metallic plates where significant plastic deformations are likely to ensue in the indented regions.

7. Conclusions

We have employed the Eshelby–Stroh formalism to study a generalized plane strain problem involving the indentation by a smooth rigid circular cylinder of a two-layer elastic composite with a through-the-width rectangular void between them. It is assumed that the void does not close during the indentation process. For a range of values of material and geometric parameters we have compared the indentation load vs. the indentation depth curves with the corresponding ones for the perfectly bonded layers. Since the slope of the indentation load vs. the indentation depth curve for a layer with a void deviates noticeably from that of the perfectly bonded one, the traditional indentation test can be used to detect voids between layers. The change in the indentation modulus increases with an increase in the void length, a decrease in the vertical distance between the void and the indenter, and an increase in Young's modulus of the layer material in the indentation direction. The change in the indentation modulus decreases as either the void moves away from the indenter or the in-plane shear modulus increases.

Acknowledgements

This work was partially supported by the ONR Grant N00014-06-1-0567 to Virginia Polytechnic Institute and State University with Dr. Y.D.S. Rajapakse as the program manager. Views expressed in the paper are those of authors and neither of the funding agency nor of VPI&SU.

Authors are indebted to Professor Senthil S. Vel of the University of Maine for providing us the source code (in MATLAB) for analyzing plane strain linear elastic problems with the Eshelby–Stroh formalism.

References

[1] Batra RC, Jiang W. Analytical solution of the contact problem of a rigid indenter and an anisotropic linear elastic layer. Int J Solid Struct 2008;45(22–23):5814–30.
[2] Cantwell WJ, Morton J. The significance of damage and defects and their detection in composite materials: a review. J Strain Anal 1992;27(1):29–42.
[3] Doebling, SW, Farrar, CR, Prima, MB, Shevitz, DW. Damage identification and health monitoring of structural and mechanical systems from changes in their vibration characteristics: a literature review. Los Alamos National Laboratory Report LA-13070-MS; 1996.

[4] Hwu C, Fan CW. Sliding punches with or without friction along the surface of an anisotropic elastic half-plane. Quar J Mech Appl Math 1998;51(Part 1):159–77.
[5] Lei GH, Ng CWW, Rigby DB. Stress and displacement around an elastic artificial rectangular hole. J Eng Mech 2001;127:880–90.
[6] Rytter A. Vibration based inspection of civil engineering structures. PhD Dissertation, Aalborg University, Department of Building Technology and Structural Engineering, Denmark; 1993.
[7] Stroh AN. Dislocations and cracks in anisotropic elasticity. Phil Mag 1958;3(30):625–46.
[8] Ting TCT. Effects of change of reference coordinates on the stress analyses of anisotropic elastic materials. Int J Solid Struct 1982;18(2):139–52.
[9] Ting TCT. Anisotropic elasticity: theory and applications. Oxford: University press; 1996.
[10] Vel SS, Batra RC. The generalized plane strain deformations of thick anisotropic composite laminated plates. Int J Solid Struct 2000;37(5):715–33.
[11] Vlassak JJ, Nix WD. Measuring the elastic properties of anisotropic materials by means of indentation experiments. J Mech Phys Solids 1994;42(8):1223–45.
[12] Vel SS, Batra RC. Analytical solutions for rectangular thick laminated plates subjected to arbitrary boundary conditions. AIAA J 1999;37:1464–73.
[13] Vel SS, Batra RC. Generalized plane strain thermoelastic deformations of laminated anisotropic plates. Int J Solid Struct 2001;38:1395–414.
[14] Vel SS, Batra RC. Analysis of piezoelectric bimorphs and plates with segmented actuators. Thin-Walled Struct. 2001;39(1):23–44.